01 Feb 2018

Probing Changes in Tilt Angle with 20 Nanoradian Resolution using an Extrinsic Fabry-Perot Interferometer-Based Optical Fiber Inclinometer

Yiyang Zhuang

Yizheng Chen

Chen Zhu

Rex E. Gerald II

et. al. For a complete list of authors, see https://scholarsmine.mst.edu/ele_comeng_facwork/3259

Recommended Citation

Y. Zhuang et al., "Probing Changes in Tilt Angle with 20 Nanoradian Resolution using an Extrinsic Fabry-Perot Interferometer-Based Optical Fiber Inclinometer," *Optics Express*, vol. 26, no. 3, pp. 2546-2556, OSA - The Optical Society, Feb 2018.
The definitive version is available at https://doi.org/10.1364/OE.26.002546

Research Article | Vol. 26, No. 3 | 5 Feb 2018 | OPTICS EXPRESS 2546
Optics EXPRESS

Probing changes in tilt angle with 20 nanoradian resolution using an extrinsic Fabry-Perot interferometer-based optical fiber inclinometer

YIYANG ZHUANG,[1,3] YIZHENG CHEN,[1,3] CHEN ZHU,[1] REX E. GERALD II,[2] and JIE HUANG[1,*]

[1]*Department of Electrical and Computer Engineering, Missouri University of Science and Technology, Rolla, MO 65409, USA*
[2]*American Inventor Institute, Willow Spring, IL 60480, USA*
[3]*These authors contributed equally to this work*
**jieh@mst.edu*

Abstract: In this paper, we introduce and demonstrate a novel optical fiber extrinsic Fabry-Perot interferometer (EFPI) for tilt measurements with 20 nrad resolution. Compared with in-line optical fiber inclinometers, an extrinsic sensing structure is used in the inclinometer reported herein. Our design greatly improves on the tilt angle resolution, the temperature stability, and the mechanical robustness of inclinometers with advanced designs. An EFPI cavity, which is formed between endfaces of a suspended rectangular mass block and a fixed optical fiber, is packaged inside a rectangular container box with an oscillation dampening mechanism. Importantly, the two reflectors of the EFPI sensor remain parallel while the cavity length of the EFPI sensor meters a change in tilt. According to the Fabry-Perot principle, the change in the cavity length can be determined, and the tilt angle of the inclinometer can be calculated. The sensor design and the measurement principle are discussed. An experiment based on measuring the tilt angle of a simply-supported 70-cm beam induced by a small load is presented to verify the resolution of our prototype inclinometer. The experimental results demonstrate significantly higher resolution (ca. 20 nrad) compared to commercial devices. The temperature cross-talk of the inclinometer was also investigated in a separate experiment and found to be 0.0041 μrad /°C. Our inclinometer was also employed for monitoring the daily periodic variations in the tilt angle of a windowsill in a cement building caused by local temperature changes during a five-day period. The multi-day study demonstrated excellent stability and practicability for the novel device. The significant inclinometer improvements in differential tilt angle resolution, temperature compensation, and mechanical robustness also provide unique opportunities for investigating spatial-temporal modulations of gravitational fields.

OCIS codes: (120.2230) Fabry-Perot; (060.2370) Fiber optics sensors; (000.2780) Gravity.

References and links

1. Y.-T. Ho, A.-B. Huang, and J.-T. Lee, "Development of a fibre Bragg grating sensored ground movement monitoring system," Meas. Sci. Technol. **17**(7), 1733–1740 (2006).
2. H.-F. Pei, J.-H. Yin, H.-H. Zhu, C.-Y. Hong, W. Jin, and D.-S. Xu, "Monitoring of lateral displacements of a slope using a series of special fibre Bragg grating-based in-place inclinometers," Meas. Sci. Technol. **23**(2), 025007 (2012).
3. S. Vurpillot, G. Krueger, D. Benouaich, D. Clément, and D. Inaudi, "Vertical deflection of a pre-stressed concrete bridge obtained using deformation sensors and inclinometer measurements," ACI Struct. J. **95**(5), 518–526 (1998).
4. D. W. Ha, H. S. Park, S. W. Choi, and Y. Kim, "A wireless MEMS-based inclinometer sensor node for structural health monitoring," Sensors (Basel) **13**(12), 16090–16104 (2013).
5. Y.-G. Lee, H.-K. Jang, D.-H. Kim, and C.-G. Kim, "Development of a mirror mounted fiber optic inclinometer," Sensor Actuat, A-Phys. **184**, 46–52 (2012).

#312727 https://doi.org/10.1364/OE.26.002546
Journal © 2017 Received 3 Nov 2017; revised 18 Jan 2018; accepted 18 Jan 2018; published 24 Jan 2018
Corrected: 29 January 2018

Optics EXPRESS

6. H.-N. Li, D.-S. Li, and G.-B. Song, "Recent applications of fiber optic sensors to health monitoring in civil engineering," Eng. Struct. **26**(11), 1647–1657 (2004).
7. L.-Y. Shao and J. Albert, "Compact fiber-optic vector inclinometer," Opt. Lett. **35**(7), 1034–1036 (2010).
8. O. Frazão, R. Falate, J. L. Fabris, J. L. Santos, L. A. Ferreira, and F. M. Araújo, "Optical inclinometer based on a single long-period fiber grating combined with a fused taper," Opt. Lett. **31**(20), 2960–2962 (2006).
9. L. Amaral, O. Frazão, J. Santos, and A. L. Ribeiro, "Fiber-optic inclinometer based on taper Michelson interferometer," IEEE Sens. J. **11**(9), 1811–1814 (2011).
10. T. Osuch, K. Markowski, A. Manujło, and K. Jędrzejewski, "Coupling independent fiber optic tilt and temperature sensor based on chirped tapered fiber Bragg grating in double-pass configuration," Sensor Actuat. A-Phys. **252**, 76–81 (2016).
11. C.-L. Lee, W.-C. Shih, J.-M. Hsu, and J.-S. Horng, "Asymmetrical dual tapered fiber Mach-Zehnder interferometer for fiber-optic directional tilt sensor," Opt. Express **22**(20), 24646–24654 (2014).
12. H. Bao, X. Dong, L.-Y. Shao, C.-L. Zhao, C. Chan, and P. Shum, "Temperature-insensitive 2-D pendulum clinometer using two fiber Bragg gratings," IEEE Photonics Technol. Lett. **22**(12), 863–865 (2010).
13. H. Bao, X. Dong, C. Zhao, L.-Y. Shao, C. C. Chan, and P. Shum, "Temperature-insensitive FBG tilt sensor with a large measurement range," Opt. Commun. **283**(6), 968–970 (2010).
14. B.-J. Peng, Y. Zhao, Y. Zhao, and J. Yang, "Tilt sensor with FBG technology and matched FBG demodulating method," IEEE Sens. J. **6**(1), 63–66 (2006).
15. S. Liu, N. Liu, M. Hou, J. Guo, Z. Li, and P. Lu, "Direction-independent fiber inclinometer based on simplified hollow core photonic crystal fiber," Opt. Lett. **38**(4), 449–451 (2013).
16. Q. Rong, X. Qiao, T. Guo, H. Yang, Y. Du, D. Su, R. Wang, D. Feng, M. Hu, and Z. Feng, "Orientation-dependant inclinometer based on intermodal coupling of two-LP-modes in a polarization-maintaining photonic crystal fiber," Opt. Express **21**(15), 17576–17585 (2013).
17. LIGO Scientific Collaboration and Virgo Collaboration, "Observation of gravitational waves from a binary black hole merger," Phys. Rev. Lett. **116**(6), 061102 (2016).
18. M. Schmidt, B. Werther, N. Fuerstenau, M. Matthias, and T. Melz, "Fiber-Optic Extrinsic Fabry-Perot Interferometer Strain Sensor with <50 pm displacement resolution using three-wavelength digital phase demodulation," Opt. Express **8**(8), 475–480 (2001).
19. Y. Huang, T. Wei, Z. Zhou, Y. Zhang, G. Chen, and H. Xiao, "An extrinsic Fabry–Perot interferometer-based large strain sensor with high resolution," Meas. Sci. Technol. **21**(10), 105308 (2010).
20. B. H. Lee, Y. H. Kim, K. S. Park, J. B. Eom, M. J. Kim, B. S. Rho, and H. Y. Choi, "Interferometric fiber optic sensors," Sensors (Basel) **12**(3), 2467–2486 (2012).
21. C. Zhu, Y. Chen, Y. Du, Y. Zhuang, F. Liu, R. E. Gerald, and J. Huang, "A displacement sensor with centimeter dynamic range and submicrometer resolution based on an optical interferometer," IEEE Sens. J. **17**(17), 5523–5528 (2017).
22. Y. Du, Y. Chen, C. Zhu, Y. Zhuang, and J. Huang, "An embeddable optical strain gauge based on a buckled beam," Rev. Sci. Instrum. **88**(11), 115002 (2017).
23. C. Zhu, Y. Chen, Y. Zhuang, Y. Du, R. E. Gerald II, Y. Tang, and J. Huang, "An optical interferometric triaxial displacement sensor for structural health monitoring: characterization of sliding and debonding for a delamination process," Sensors (Basel) **17**(11), 2696 (2017).
24. Y. Du, Y. Chen, Y. Zhuang, C. Zhu, F. Tang, and J. Huang, "Probing nanostrain via a mechanically designed optical fiber interferometer," IEEE Photonics Technol. Lett. **29**(16), 1348–1351 (2017).
25. Wunderground.com, "Rolla, MO Forecast | weather underground ", retrieved October 25th, 2017, https://www.wunderground.com/weather/us/mo/rolla/65401.

1. Introduction

Inclinometers purposed for tilt measurements have attracted considerable attention for structural health monitoring and warning of impending natural disasters such as landslides and earthquakes [1–3]. The concept behind a typical inclinometer is that it measures variations in tilt angle generated by the behavior of a pendulum subject to a gravitational field [4].

For applications in harsh environments, modern inclinometers require high resolution and long measurement times to precisely and continuously measure variations in the tilt angle. Advanced applications require that inclinometers function in remote and unreachable places, requiring capabilities such as long-distance transmission without loss and interference from electromagnetic sources, resistance to hazardous environments, etc [5]. The conventional electrolytic inclinometers, which have been widely used in practical applications, suffer from large transmission loss and electromagnetic interferences. However, fiber optic sensors could be promising candidates for inclinometers owing to their unique advantages such as immunity to electromagnetic fields, low transmission losses, high accuracy, the possibility of remote operation, robustness, etc [6]. In recent years, a variety of fiber optic inclinometers have been

Optics EXPRESS

reported and developed [7–16]. The majority of the previously reported fiber optic inclinometers are fabricated in-line (i.e., the sensor is fabricated using a piece of optical fiber), and the principles of sensing are based on wavelength or intensity modulation of the input signal caused by bending the fiber optic sensors as demonstrated for fiber tapers [7–11], fiber Bragg gratings (FBG) [12–14], and photonic crystal fibers [15, 16].

Although the inclinometers mentioned above show great capability in tilt measurement, there exist several drawbacks. For fiber taper-based fiber optic inclinometers, using a fiber taper can greatly reduce the mechanical strength of the sensor structure, which is too delicate for harsh environment. For FBG-based fiber optic inclinometers, one or more FBGs will be attached to a vertical cantilever-based pendulum and used to measure the strain variations of the cantilever caused by gravity-induced bending [12–14]. However, FBG-based inclinometers suffer from unwanted mechanical frictions, rotations, and instabilities because the force transfer from the cantilever to the FBGs is complicated. Furthermore, the accuracy of the FBG-based inclinometers will diminish in a vibrationally-unstable environment because the cantilever will experience a mechanical resonance [14]. Also, the resolution for all the aforementioned fiber optic inclinometers is less than 0.001° (17.5 μrad) [7–16], which is not sufficient for some applications like gravitational field measurements that require extremely high-precision tilt measurements [17].

Compared to the in-line structure fiber optic sensors, the extrinsic optical fiber sensors can overcome the disadvantage of low mechanical strength because the optical fiber only served as a transceiver of light signals. Recently, Lee et al. reported a packaged fiber optic inclinometer using a moveable transmissive grating panel, reflective mirror, and optical fibers as transceivers [5]. Their reported inclinometer achieved a full-scale measurement range of ± 90°. But, the fabrication process for the transmissive grating panel is complicated. Meanwhile, a widely used interferometric sensor, the extrinsic Fabry-Perot interferometer (EFPI), has the merit of displacement and strain measurements [18–24]. An EFPI is formed by the endface of an optical fiber and an external reflecting surface. The cavity length of the EFPI (i.e., the distance between the two reflecting surfaces) can be accurately measured from the reflection spectrum [18]. Therefore, with proper structure design and packaging, an inclinometer based on EFPI displacement measurements will be able to take advantage of high resolution, and it could be considered as a good candidate for tilt measurements.

In this paper, we report a high resolution EFPI-based optical fiber inclinometer for tilt measurements. The reported inclinometer consists of an EFPI sensor packaged inside a rectangular metal container box. The sensor design and the measurement principles are discussed in Section II. An example application experiment based on measuring the tilt angle of a simply supported 70-cm beam, induced by small incremental loads (2.000g), is presented in Section III to verify the resolution of the novel inclinometer. Our results demonstrate a high resolution of 16.7 nrad. The novel inclinometer was also employed throughout five days to monitor the variations in the tilt angle of a windowsill caused by daily (cyclic) temperature changes.

2. Sensor design and measurement principles

A schematic diagram of a partial side view of the inclinometer is illustrated in Fig. 1(a). The EFPI sensor is fabricated and packaged in a rectangular metal container box. The EFPI sensor consists of two parts: the mass block part and the optical fiber module. The rectangular mass block is flexibly connected to the top plate of the rectangular container box by two stainless steel multi-strand ropes of the same length. The distance between two connection points on the mass block and the corresponding connection points on the top plate are identical. The four connection points are contained in a common plane, and the stainless steel multi-strand ropes are perpendicular to the horizontal plane of the inclinometer. As for the optical fiber module, a segment of the optical fiber is rigidly connected to the top plate of the rectangular box by a supporting rod. The supporting rod is perpendicular to the top plate, and the endface

Optics EXPRESS

of the optical fiber is precisely adjusted to be parallel with the adjacent end face of the mass block. Therefore, the endface of the optical fiber and the adjacent endface of the mass block form an EFPI sensor. A thin layer of gold was sputtered onto the endface of the mass block to increase the reflectivity. When the inclinometer is tilted at an angle θ the two supporting ropes will remain perpendicular to the virtual horizontal Earth's ground plane as required by the Earth's gravitational field. Synchronously, the supporting rod will be tilted with the inclinometer, and the angle between the supporting rod and the ropes is the tilt angle of the inclinometer as illustrated in Fig. 1(b). The mass block will remain parallel to the top plate because the four connection points define a parallelogram. As a result, the two reflectors of the EFPI sensor will remain parallel, but the distance between the two reflector surfaces will change. The change in the tilt angle of the inclinometer can be described as follow:

$$\Delta\theta = \arcsin\left(\frac{\Delta d}{l}\right) \tag{1}$$

where Δd is the change in the cavity length of the EFPI sensor and l specifies the lengths of the ropes. When the change in the tilt angle is small, Eq. (1) can be described as:

$$\Delta\theta = \arcsin\left(\frac{\Delta d}{l}\right) \approx \frac{\Delta d}{l} \tag{2}$$

Equation (2) shows that when the change in the tilt angle is small, the sensitivity of the inclinometer, which is defined as the ratio between the change in the cavity length and the corresponding change in the tilt angle (unit: nm/nrad), is uniquely determined by the rope length. Figure 1(c) is a partial schematic diagram of the inclinometer equipped with an oscillation dampening device. A cross paddle is connected to the bottom of the mass block, and it is immersed in a damping fluid. This arrangement can physically reduce oscillations from environment-induced vibrations and thereby increase the stability of the inclinometer. The oscillation reduction can also be achieved by a magnetic dampening device. A photograph of one prototype of the inclinometer is illustrated in Fig. 1(d). To reduce the temperature cross-sensitivity of the inclinometer, during the fabrication of our inclinometer, the container box was initially backflushed with helium gas and then evacuated. Furthermore, all of the rigid components of the inclinometer, including the mass block, the supporting rod, and the rectangular box package, are made of Invar whose coefficient of thermal expansion, α_{CTE1}, is low (1.2×10^{-6}/°C). As revealed in Fig. 1(a), when the temperature of the environment fluctuates, thermal expansions/contractions will affect the size of the mass block, the container box and the ropes; these size changes will cause variations of the EFPI cavity length. The three effects result in a temperature cross-talk for the cavity length measurement. However, the contributing effects from mass block and container box will partially or completely offset each other. The result of geometrical considerations and analyses indicate that the change in the EFPI cavity length caused by a change in temperature can be described as:

$$\Delta d_t = \left(d\alpha_{CTE1} + l\theta\alpha_{CTE2}\right)\Delta T \tag{3}$$

where d is the initial cavity length of the EFPI; ΔT is the temperature change experienced by the inclinometer; θ is the tilt angle of the inclinometer to the perpendicular line and α_{CTE2} is the coefficient of thermal expansion of stainless steel.

Optics EXPRESS

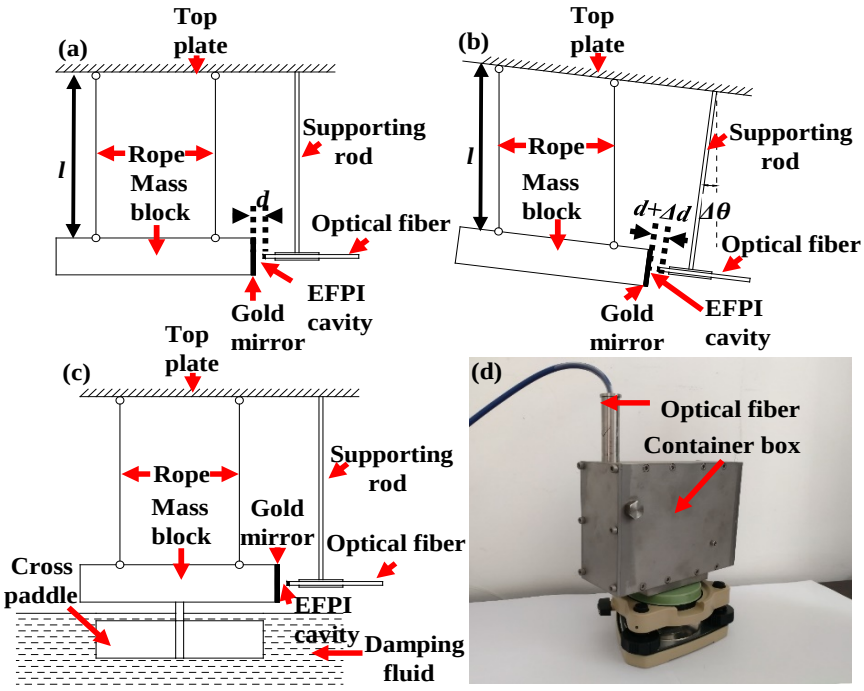

Fig. 1. Schematic diagrams and photograph of novel inclinometer. (a) Partial schematic diagram of the inclinometer. A rectangular mass block is flexibly connected to the top plate of the rectangular metal container box by two ropes with the same length. An optical fiber is rigidly connected to the top plate of the container box using a supporting rod. The EFPI sensor is formed by the combined endface of the optical fiber and the adjacent endface of the mass block. The endface of the mass block is sputtered with gold to form a highly reflective mirror surface. (b) Partial schematic diagram of the inclinometer tilted to an angle θ. The two endface reflectors of the EFPI sensor always maintain a mutual parallel disposition. (c) Partial schematic diagram of the inclinometer including an oscillation dampening device. The mass block is connected to a cross paddle which is immersed into a damping fluid. (d) Photograph of a prototype inclinometer. The inclinometer is made of Invar to reduce the temperature cross-sensitivity.

As mentioned above, the endface of the optical fiber together with the adjacent reflective endface of the mass block form the EFPI sensor with a cavity length of d. The interference signal (I_0) is given by

$$I_0 = I_1 + I_2 + 2\sqrt{I_1 I_2}\cos(\frac{4\pi nd}{\lambda} + \varphi) \tag{4}$$

where I_1 and I_2 are the light intensities reflected from the endface of the optical fiber and the adjacent gold-sputtered mirror endface of the mass block, respectively; φ is the initial phase difference between the light waves reflected from the two reflectors; n is the refractive index of the cavity which is about 1 and λ is the wavelength of the incident light. When the variables inside the cosine function of Eq. (4) are equal to a multiple of 2π, a constructive interference results. In the wavelength spectrum of the interference signal, the space between two adjacent peaks, defined as the free spectrum range (FSR), can be expressed as:

$$FSR = \frac{\lambda_c^{\ 2}}{2d} \tag{5}$$

where λ_c is the center wavelength of the interference spectrum. So, the cavity length can be demodulated by determining the FSR of the interference spectrum. When the inclinometer is

Optics EXPRESS

tilted, the cavity length of the EFPI will experience a change. The change in cavity length can be evaluated by:

$$\Delta d = \frac{\lambda_c^{\,2}\Delta FSR}{2FSR_0FSR_1} \tag{6}$$

where FSR_0 and FSR_1 are the values of FSR before and after the tilt, respectively; and, ΔFSR is the difference between FSR_0 and FSR_1. If the mass block module tilts clockwise, the cavity length of the EFPI will decrease. And, if the mass block module tilts counterclockwise, the cavity length of the EFPI will increase. Hence, the sign of ΔFSR can be used to determine the direction of tilt.

Concerning the demodulation principle described above, variations of the cavity length of the EFPI can be determined. It should be noted that no matter how great the tilt angle is, the endface of the optical fiber will always remain parallel to the adjacent reflective endface of the mass block. So, the tilt angle can be measured if the cavity length change is within a proper range (i.e., the cavity length of the EFPI is approximately within 0 to 1 mm). More significantly, the measurement range and sensitivity of the inclinometer can be adjusted by simply changing the lengths of the stainless steel multi-strand ropes, and adjusting the initial cavity length of the EFPI during the fabrication of the inclinometer. For example, if the lengths of the stainless steel multi-strand ropes are 1.000 cm and the initial cavity length of the EFPI is 500.000 μm, then the measurement range and sensitivity of the inclinometer are calculated to be ± 50 mrad and 0.01 nm/nrad (cavity length change/tilt angle change), respectively. This adjustability feature expands the capability of our inclinometer for different tilt measurement applications.

3. Experimental results and discussions

To verify the resolution of the prototype inclinometer, a verification experiment based on measuring the tilt angle of a simply-supported beam under external load was designed and tested. The schematic diagram of the test experiment setup is illustrated in Fig. 2(a). The beam is made of stainless steel. The size of the beam is 700.0 mm × 50.0 mm × 8.0 mm. The distance between each support point and the respective end of the beam is 100.0 mm, so the effective length of the beam is 500.0 mm. The inclinometer is placed at the same position as one of the support points. Several copper washers were placed on the beam at the center position to provide the necessary load to cause the beam to bend and, therefore, tilt the beam at both support points. To prevent the copper washers from moving, a cylindrical post was attached to the center of the beam and used to position and secure the copper washers.

At the support points, very small tilt angles can be calculated using:

$$\theta = \frac{Fl_s^{\,2}}{16EI} \tag{7}$$

where F is the load applied to the center of the beam; l_s is the length between the two support points; E is Young's modulus for the stainless steel beam material used in the experiment (about 200 GPa), and I is the moment of inertia. The test measurement setup for the inclinometer apparatus is illustrated in Fig. 2(b). A wavelength interrogator (Micron Optics SM125) which integrates a swept laser, a photodetector, and an optical fiber coupler was used as the source and demodulation device. The incident light was directed into the inclinometer then reflected back to the interrogator through the single-mode fiber. The reflected spectrum was obtained by sweeping the wavelength of the laser (from 1510 nm to 1590 nm) and recording the corresponding intensities of the reflected signals. A personal computer was connected to the SM125 to record and analyze the interference spectra using a LabVIEW program developed in our lab. Detailed descriptions of the measurement apparatus can be found in our recent work [21–24].

Optics EXPRESS

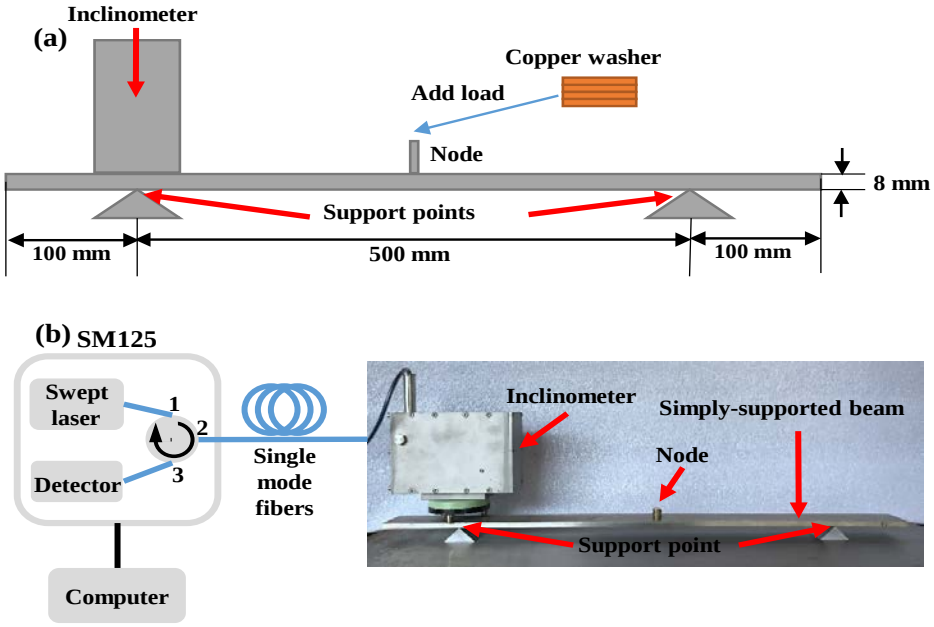

Fig. 2. Experimental apparatus for verifying the inclinometer using a simply-supported beam. (a) Schematic cross-section diagram of the tilt angle verification experiment based on a simply-supported beam. The inclinometer is placed at the location of a support point. Copper washers were used to provide the load for tilting the beam. (b) A photograph of the experimental test setup and the inclinometer. Schematic diagram of the test measurement setup that is coupled to the inclinometer. A Micron Optics SM125 was used as the source and demodulation device. A personal computer was used to analyze the interference spectra.

Figure 3(a) shows the interference spectrum of the EFPI based inclinometer without a load applied to the beam. The averaged FSR of the spectrum is 5.071 nm, corresponding to the initial EFPI cavity length of 236.871 μm. In our verification experiment, the cavity length was measured for 55 minutes. During the series of tilt experiments, a copper washer was placed on the post of the beam every five minutes, and every minute the interference spectrum was recorded. Hence, for each load, five interference spectra were recorded to calculate the cavity length of the EFPI sensor. The weight of each copper washer is 2.000 g. The lengths of the ropes were set to 6.000 cm in the prototype inclinometer and the dynamic range of the inclinometer was calculated to be ± 8.333 mrad. A silicone fluid with 500000 cSt was used as the damper fluid. The size for each paddle is 33 mm × 11 mm × 1 mm in the prototype inclinometer. According to Eq. (6), when a copper washer was placed on the center post of the beam, it would induce a tilt angle of magnitude 0.717 μrad to the beam at each support point. The total load ranged from 0 to 20.000 g, corresponding to a tilt angle range from 0 to 7.170 μrad. The verification results for the inclinometer are shown in Fig. 3(b). The left vertical axis represents the measured cavity length of the EFPI sensor, and the right vertical axis represents the measured tilt angle, which was calculated from Eq. (2). In Fig. 3(b), 0.717 μrad steps increments of the tilt angle can be easily distinguished. The measurement setup based on the SM125 can achieve a resolution of 1.0 nm for the cavity length. Thus, the EFPI based inclinometer can achieve a measurement resolution of 16.7 nrad according to Eq. (2). Multiple measurements of the cavity length, and the corresponding tilt angle recorded when the applied load was 16.000 g are presented as an inset in Fig. 3(b). We calculated that the standard deviation of the tilt angle measurement uncertainty is 11.2 nrad. The measured variations are due to environmental perturbations such as temperature fluctuations, experimental setup vibrations, etc. The measured tilt angle as a function of applied theoretical tilt angle is shown in Fig. 3(c). The linear fit (red line) produced an R-

Optics EXPRESS

square of 1.000, indicating an excellent correlation and linearity between the applied tilt angle and measured tilt angle. The slope and the intercept of the linear fit result reveal the difference between the applied tilt angle and measured tilt angle. The reason for the difference was that we use the angle calculated from Eq. (7) as the applied tilt angle, but the calculation was based on the assumptions that the tilt angle of our inclinometer was equal to the tilt angle of the beam at the support point, and the load was concentrated at the center of the beam. The error introduced by the mathematical approximation in Eq. (2) is much smaller than the deviation of the measured angle, which can be neglected. Importantly, the numerical value of the slope (near unity) for a linear fit to the data in Fig. 3(c) provides strong and independent evidence for the application of sound physics principles used in the design and operation of the inclinometer because the comparison is made between absolute tilt angles that are derived from independent and fundamentally different physics; one angle is derived from the deformation of a rigid beam and the other from the basic geometry considerations of a parallelogram-mediated gap.

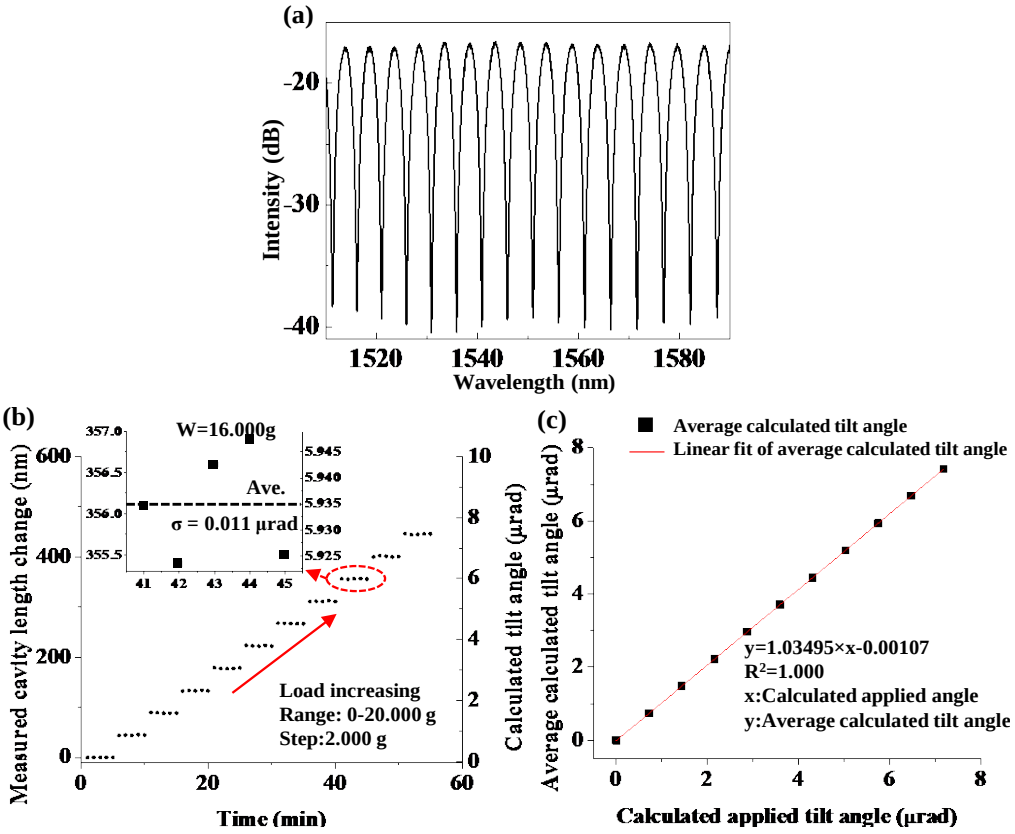

Fig. 3. Experimental data for verifying the inclinometer using a simply-supported beam. (a) Interference spectrum of the EFPI-based inclinometer without a load applied to the beam. The spectrum was recorded from 1510 nm to 1590 nm. (b)The verification result of the EFPI-based inclinometer. The measured change in the cavity length and the calculated tilt angle are shown as a function of time. Every five minutes, the load was increased by 2.000 g, and every minute the interference spectrum was recorded. The inset shows the change in the cavity length and the measured tilt angle from 41 to 45 minutes. (c) The average calculated tilt angle correlated to the calculated applied tilt angle and a linear fit was the result. The equation for the linear fit is y = 1.03495 × x-0.00107, where *y* represents average calculated tilt angle and *x* represents calculated applied tilt angle.

Optics EXPRESS

The response of our prototype inclinometer to variations in temperature was investigated in a separate experiment. The experimental setup is illustrated in Fig. 4(a). The inclinometer was placed inside a temperature-controlled box. Each side of the box was filled with insulating foam. A cylindrical rod fused silica base was used at the bottom of the box, and the prototype inclinometer was fixed on the top of the base because the fused silica has a more uniform mechanical deformation thermal expansion effect than the insulation foam. It is very important to note that the inclinometer is suspended inside the oven by resting on a cylindrical rod of fused silica that is in direct contact with the floor of the laboratory and has no contact with the oven. Every hour, the temperature inside the box was increased by 10 °C. After 50 minutes of temperature stabilization, the interference signal was recorded ten times in 10 minutes. The total temperature range is from 0 to 50 °C. The experimental results are demonstrated in Figs. 4(b) and 4(c).

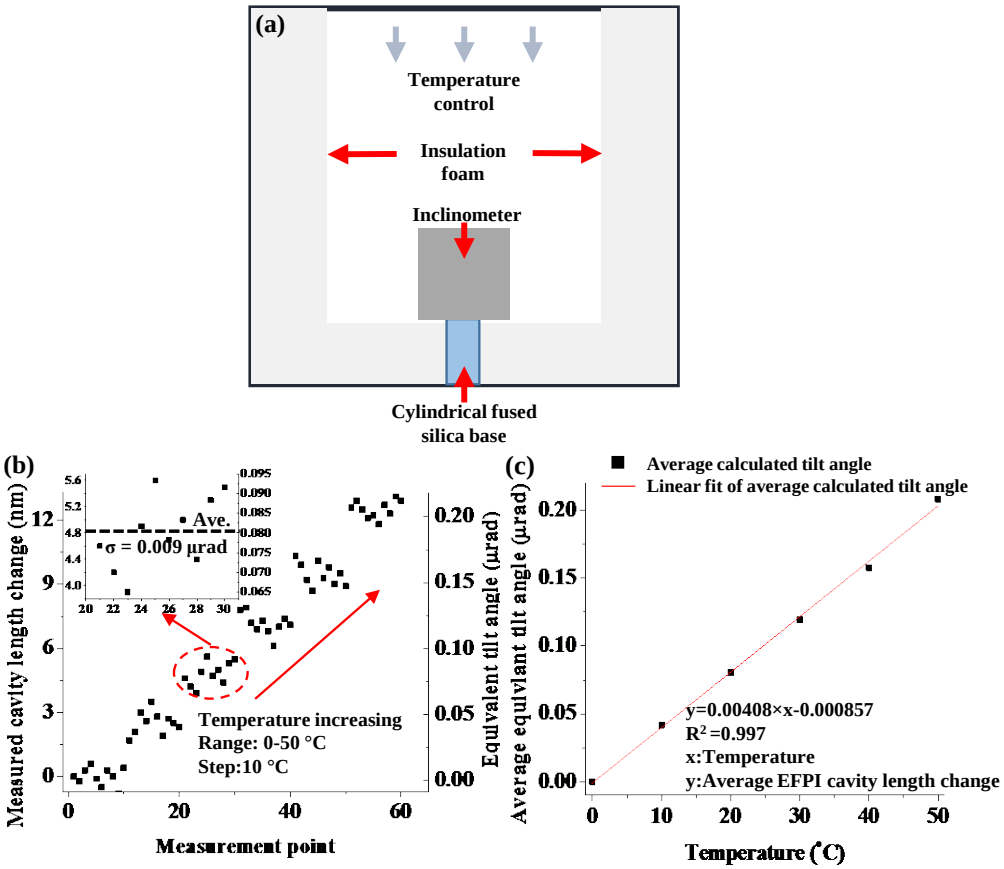

Fig. 4. Experimental setup and results for quantifying the effects of temperature on the inclinometer. Note that the inclinometer is suspended inside the oven by resting on a cylindrical rod of fused silica that is in direct contact with the floor of the laboratory and has no contact with the oven. (a) Experimental setup for testing the response of the prototype inclinometer to variations in temperature. The inclinometer was placed inside a temperature-controlled box filling with insulating foam. The inclinometer was placed on a solid cylindrical rod base of fused silica positioned at the bottom of the box. (b) EFPI cavity length change derived from all of the recorded interference signals as a function of temperature. The temperature in the temperature-controlled box was increased from 0 to 50 °C with a step size of 10 °C. (c) Average equivalent tilt angle change as a function of temperature. The linear fit result is shown as a red line. The slope of the linear fit result indicates that the temperature cross-talk for tilt angle measurements is 0.0041 μrad/°C.

Optics EXPRESS

Figure 4(b) illustrates the changes in cavity length derived from all of the recorded interference signals recorded for the experiment and the corresponding equivalent tilt angles as a function of temperature. As shown in Fig. 4(b) the overall change in the cavity length has a positive correlation with temperature. The standard deviation of the corresponding tilt angle at a constant temperature was about 9.3 nrad, which nearly matches the value presented in the inset of Fig. 3(b). The average change in the cavity length converted to a tilt angle as a function of temperature is illustrated in Fig. 4(c). The slope of the linear fit result indicates that the temperature cross-talk for the cavity length measurement is 0.258 nm/°C, corresponding to a 0.0041 μrad /°C change in tilt angle according to Eq. (2). The measured temperature cross-talk result matches well with the theoretical result, which is calculated to be 0.279 nm/°C (or 0.0044 μrad/°C) according to Eq. (3) using the initial cavity length of 232.667 μm. The influence of the temperature cross-talk is small, and it can be limited by recording the temperature data for compensation or using a proper thermal insulation device. Furthermore, a combination of the inclinometer design and a judicious choice of structural materials for the top plate and the mass block (see Fig. 1(a)) will reduce the temperature cross-talk to a negligible value. For example, a thin layer of metal with a larger coefficient of thermal expansion than Invar, like copper, can be electroplated on the side of the mass block before the gold sputtering process. In this way, the temperature cross-talk sensitivity of the inclinometer can be further reduced.

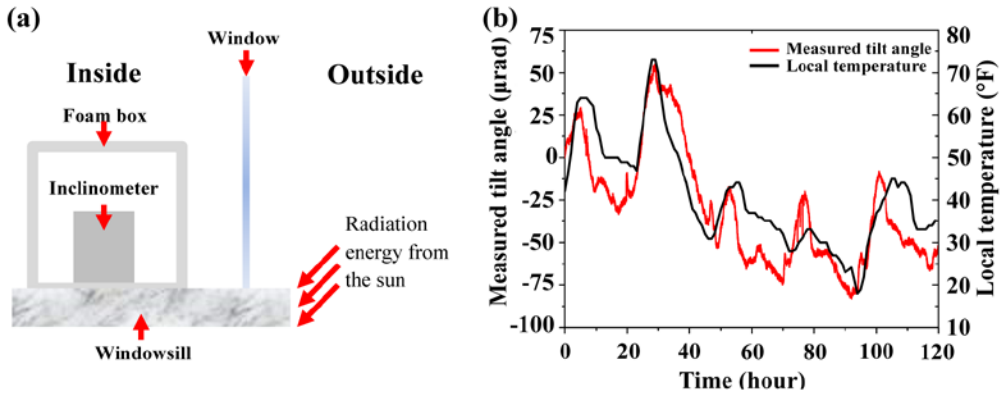

Fig. 5. A real-world application for the use of the reported inclinometer. (a) The experimental setup for monitoring variations in the tilt angle of a windowsill caused by periodic changes in the incident radiation from the sun. The inclinometer was placed on a marble windowsill, and it was sealed in a foam box, which kept the temperature inside constant and reduced the influence of temperature on the inclinometer. The window is facing south. (b) The measured tilt angle of a windowsill and local temperature change as a function of time during a five-day measurement period (from 8:00 AM on March 8th, 2017 to 8:00 AM on March 13th, 2017). An interference spectrum was recorded every ten minutes, and the cavity length was measured to calculate the tilt angle. The measured tilt angle and the published local area temperature curve follow a similar trend, showing that they are correlated. Five peaks and five valleys can be observed in both curves, corresponding approximately to 2 PM and 3 AM every day, respectively.

To verify the practicability of our prototype inclinometer, an experiment was conducted for monitoring variations in the tilt angle of a windowsill caused by periodic temperature changes. The experimental setup is illustrated in Fig. 5(a). The inclinometer was placed on a marble windowsill inside a room, and it was sealed in a foam box, which kept the inside temperature constant and reduced the temperature influences on the inclinometer. The window is facing south. The interference signal of the EFPI sensor was recorded every ten minutes during a five-day period to calculate the tilt angle as a function of time (8:00 AM March 8th, 2017 – 8:00 AM March 13th, 2017).

Optics EXPRESS

Figure 5(b) shows the experimental results for monitoring variations in the tilt angle of the windowsill and the local temperature during five days versus the experiment time. The local area temperature data was obtained from [25]. As shown in Fig. 5(b), the measured tilt angle and temperature curves map similar patterns, showing a strong correlation. Five peaks and five valleys can be observed in both plots presented in Fig. 5(b). The corresponding times for the peaks were similar, approximately 2 PM each day during the five days, while the corresponding times for the valleys occurred at approximately 3 AM each day during the five days. The results show that the tilt angles of the windowsill caused by temperature changes reached maxima in the afternoons. Interestingly, the passage of clouds during the day was also noticed by measurable changes in the tilt angle of the windowsill because the sunlight was blocked, which resulted in small temperature changes of the building and concomitant deformation in the building structure. This experiment demonstrates that our inclinometer shows high resolution and excellent stability.

4. Conclusion

In this paper, we report and demonstrate an EFPI-based fiber optic inclinometer for tilt measurements with high-resolution capability, 20 nrad, a resolution that is much higher than the resolution capabilities reported for all of the previously published fiber optic inclinometers and commercially available inclinometers. Compared to in-line fiber optic inclinometers, the extrinsic sensing motif was used in our prototype inclinometer. Our inclinometer consists of an EFPI-based sensor packaged inside a rectangular container box. A rectangular mass block is flexibly connected to the top plate of the rectangular container box by two stainless steel multi-strand ropes of the same lengths. An optical fiber is rigidly connected to the top plate of the rectangular container box by a supporting rod. Therefore, the endface of the optical fiber and the adjacent mirror endface of the mass block serve as the two reflectors of an EFPI sensor. To reduce the effects of oscillations, the rectangular mass block is connected to a cross paddle, which is immersed in a damping fluid. After tilting, the two endface reflectors of the EFPI sensor will remain parallel while the cavity length of the EFPI sensor will experience a change. According to the Fabry-Perot principle, the change in the cavity length can be determined, and the tilt angle of the inclinometer can be calculated. The sensor design and the measurement principles are discussed. An experiment based on measuring the tilt angle of a simply-supported beam induced by a small load is presented to verify the resolution of the prototype inclinometer, demonstrating high resolution. The temperature cross-talk for tilt angle measurements is 0.0041 μrad /°C, which is small compared with the resolution of the inclinometer. The prototype inclinometer was also used for monitoring variations in the tilt angle of a windowsill caused by periodic changes in the incident radiation from the sun during a five-day period, and it demonstrated excellent robustness, stability, and practicality. The sensitivity and dynamic range of the inclinometer can be flexibly configured by simply changing the length of the rope. The resolution of 20 nrad that we achieved with our inclinometer provides opportunities to use the novel device for investigating subtle distortions in the gravitational field caused by distant planets, or for monitoring and forecasting distortions in the earth's mantle, which lead to natural disasters like earthquakes.

Funding

University of Missouri Research Board.